SenseBack - An implantable system for bidirectional neural interfacing

SenseBack - An Implantable System for Bidirectional Neural Interfacing

Ian Williams, *Member, IEEE*, Emma Brunton, *Member, IEEE*, Adrien Rapeaux, *Student Member, IEEE*, Yan Liu, *Member, IEEE*, Song Luan, *Member, IEEE*, Kianoush Nazarpour, *Senior Member, IEEE*, and Timothy G. Constandinou, *Senior Member, IEEE*

***Abstract*—Chronic *in-vivo* neurophysiology experiments require highly miniaturized, remotely powered multi-channel neural interfaces which are currently lacking in power or flexibility post implantation. In this article, to resolve this problem we present the SenseBack system, a post-implantation reprogrammable wireless 32-channel bidirectional neural interfacing that can enable chronic peripheral electrophysiology experiments in freely behaving small animals. The large number of channels for a peripheral neural interface, coupled with fully implantable hardware and complete software flexibility enable complex *in-vivo* studies where the system can adapt to evolving study needs as they arise. In complementary *ex-vivo* and *in-vivo* preparations, we demonstrate that this system can record neural signals and perform high-voltage, bipolar stimulation on any channel. In addition, we demonstrate transcutaneous power delivery and Bluetooth 5 data communication with a PC. The SenseBack system is capable of stimulation on any channel with ±20 V of compliance and up to 315 μA of current, and highly configurable recording with per-channel adjustable gain and filtering with 8 sets of 10-bit ADCs to sample data at 20 kHz for each channel. To the best of our knowledge this is the first such implantable research platform offering this level of performance and flexibility post-implantation (including complete reprogramming even after encapsulation) for small animal electrophysiology. Here we present initial acute trials, demonstrations and progress towards a system that we expect to enable a wide range of electrophysiology experiments in freely behaving animals.**

Manuscript received June 18, 2020; revised August 11, 2020; accepted September 3, 2020. Date of publication September 10, 2020; date of current version October 15, 2020. This work was supported by the Engineering and Physical Sciences Research Council (EPSRC), U.K. under Grants EP/M025977/1, EP/N023080/1, EP/M020975/1, EP/R004242/1, and EP/K015060/1. This article was recommended by Associate Editor Dr. Leanne Lai Hang Chan. *(Corresponding author: Ian Williams.)*

Ian Williams is with the Department of Electrical and Electronic Engineering, Imperial College London, SW7 2BT London, U.K. (e-mail: i.williams10@imperial.ac.uk).

Emma Brunton was with the School of Engineering, Newcastle University, NE1 7RU Newcastle upon Tyne, Tyne and Wear, U.K. (e-mail: emma.brunton@newcastle.ac.uk).

Adrien Rapeaux and Timothy G. Constandinou are with the Department of Electrical and Electronic Engineering and Care Research & Technology Centre, U.K. Dementia Research Institute, Imperial College London, SW7 2BT London, U.K. (e-mail: adrien.rapeaux13@imperial.ac.uk; t.constandinou@imperial.ac.uk).

Yan Liu is with the Department of Micro-Nano Electronics, Shanghai Jiaotong University, Shanghai 200240, P. R. China (e-mail: yan.liu06@imperial.ac.uk).

Song Luan is with the DNA Nudge Ltd, Imperial College White City Campus, W12 0BZ London, U.K. (e-mail: s.luan@imperial.ac.uk).

Kianoush Nazarpour is with the School of Informatics, The University of Edinburgh, EH8 9AB Edinburgh, U.K. (e-mail: kianoush.nazarpour@ed.ac.uk).

Color versions of one or more of the figures in this article are available online at https://ieeexplore.ieee.org.

Digital Object Identifier 10.1109/TBCAS.2020.3022839

***Index Terms*—Bioelectronics, neural interfacing, prosthetics, rodent.**

I. Introduction

THERE is hope that advanced prosthetics could one day offer millions of people with limb difference the prospect of greatly increased functional recovery [1]. However, a technological gulf, as well as gaps in our understanding of the fundamental neuroscience remain between that future goal and the current state of the art [2]–[5]. Recognising this, we sought to develop technologies that could provide artificial sensation from a prosthetic limb with a particular focus on proprioceptive and tactile feedback [2], [6]–[8]. Such systems would not only revolutionize the field of limb prosthetics and interfacing with the peripheral nervous system (PNS) can offer a new technological paradigm for interfacing with the autonomic nervous system, paving the way for future bioelectronic medicine [9]–[13].

The consensus is that electrical neural interfaces to the PNS offer the best *near-term* prospect for highly capable and naturalistic sensory feedback [14], [15]. However, several major challenges were identified [16]–[18] including: the trade off between the selectivity and long term stability of electrodes; targeting of axons innervating specific areas of the body and specific receptor types; methods of modulating the neural signals to provide high quality sensation; and a low power implantable device capable of delivering the stimulation patterns to a selective electrode interface. A multi-pronged approach to address these challenges was pursued with a key element being the development of a chronic, small-rodent neuroscience platform to investigate and demonstrate advances [19]–[21]. Chronic operation was desired both because of the experimental opportunities it provides and because of the need to investigate long-term stability [16].

Despite decades of documented work, chronic neurotechnology experiments with freely behaving rodents still present many difficulties. Tethered interfaces, which are used in many experiments, restrict behaviours and the range of experiments that can be performed, and percutaneous connections are associated with an increased risk of infection [22]. As such fully implanted solutions are highly desirable; but this in turn drives a need for wireless data communication and, depending on experiment duration, wireless transcutaneous power transmission. An implanted solution also imposes drastic size and weight restrictions. Previous comparable systems [23]–[26] have approached

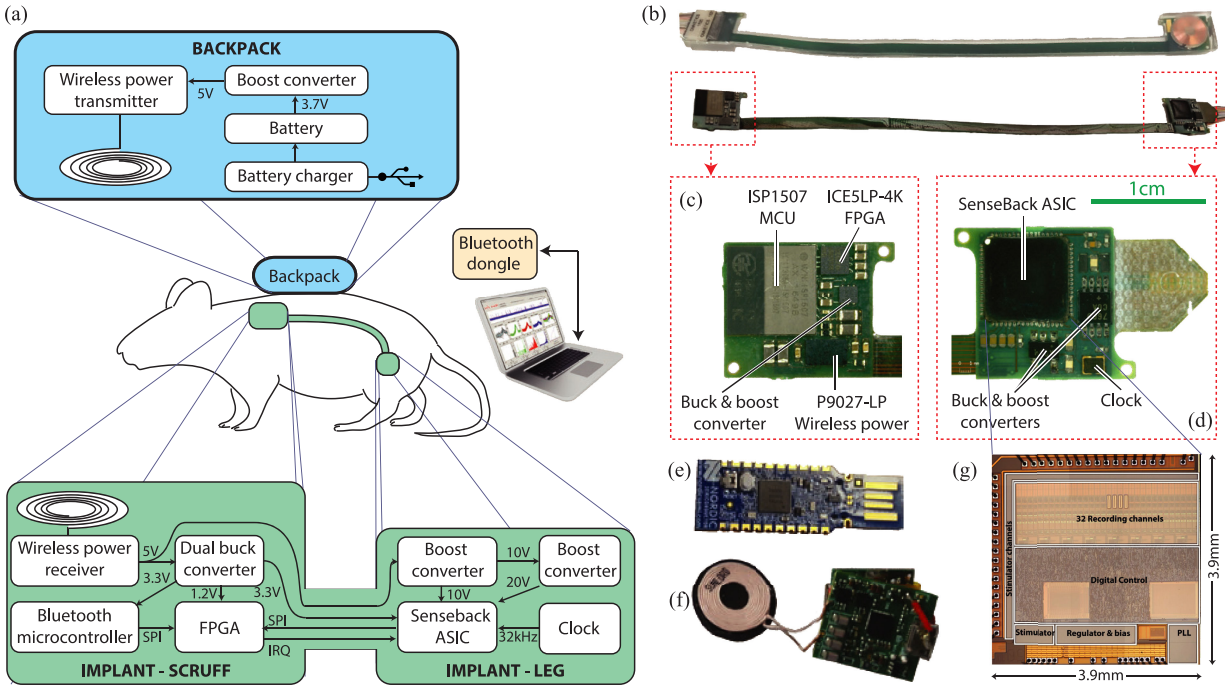

Fig. 1. SenseBack system: (a). The block diagram of the overall system; (b). The SenseBack implant pre- and post-encapsulation; (c) and (d). Zoom in of the wireless interface (located in the neck scruff) and the neural interface (implanted near the nerve of interest) nodes; (e). The PC dongle Bluetooth transceiver; (f). The backpack electronics and battery; and (g). The bare die of the ASIC chip.

these challenges by implementing a very low number of channels of either stimulation or recording, and many have also been too large for small rodents. Our system offers groundbreaking flexibility, with 32 channels of highly configurable stimulation and individually configurable recording in a miniature package; encapsulated in medical grade silicone suitable for six months implantation. The system is further enhanced by the inclusion of underutilised processing hardware (both microcontroller and FPGA resource) combined with fully wirelessly upgradeable firmware (even post-encapsulation and implantation), opening up the possibility for an experimenter to radically alter the system purpose at any point in time.

The SenseBack project[1] was conceived to develop enabling technologies to restore sensory feedback in assistive devices, such as prosthetic hands (hence the term coined 'Sense-Back') [1], [6]–[8], [27]–[30]. A key aim here has been to create new research tools that are capable of bidirectional neural interfacing in chronic rodent experiments. This would provide the opportunity to sense and stimulate neural or muscular activity and potentially provide closed-loop feedback. The work described herein details the system integration of this platform.

This paper reports our progress to date in designing, building and testing the SenseBack system, which comprises three main modules: 1) a controlling PC (with Bluetooth 5 interface dongle); 2) a backpack containing a battery, battery charger and an inductive wireless power transmitter; and 3) an implant constructed on a single strip of rigid-flex PCB with a rigid area at each end, where components are mounted. One end of the implant is designed to handle the wireless transfer of data and power, while the other end performs the neural interfacing using an Application Specific Integrated Circuit (ASIC) and supporting electronics. Power is supplied through an inductive wireless link in the animal's scruff of the neck and bidirectional data flow is over a 2 Mbps Bluetooth 5 connection. This paper provides insight into the numerous challenges and trade-offs present in transitioning a neural interface chip into a full fledged implantable system, and provides an example solution to them. Pre-manufacture simulations of the chip and a brief account of the system design were presented previously [6], [30]. Fig. 1(a) shows the block-diagram of the system.

[1]SenseBack project website: http://www.senseback.com

II. Methods

A. Implant

The SenseBack implant was implemented on a flex-rigid PCB consisting of two rigid nodes at either end of a 100 μm-thin flexible polyimide strip, which carries power and data between the two nodes, as shown in Fig. 1(b)–(d). One end of the implant is designed to position in the scruff of the neck of the animal and interfaces wirelessly with the outside circuit, in a backpack, for power and data transmission. The other end can be routed to any limb to interface with the neural tissue. The system was targeted at rat experiments and so the size of the scruff and hindlimb nodes was constrained to less than 15 $\times$ 15 mm following exploratory dissections of rodents euthanised for other unrelated projects.

The two key elements of the implant are the SenseBack neural interface ASIC and the NRF52832 bluetooth microcontroller (MCU). These are supported by a Field Programmable Gate

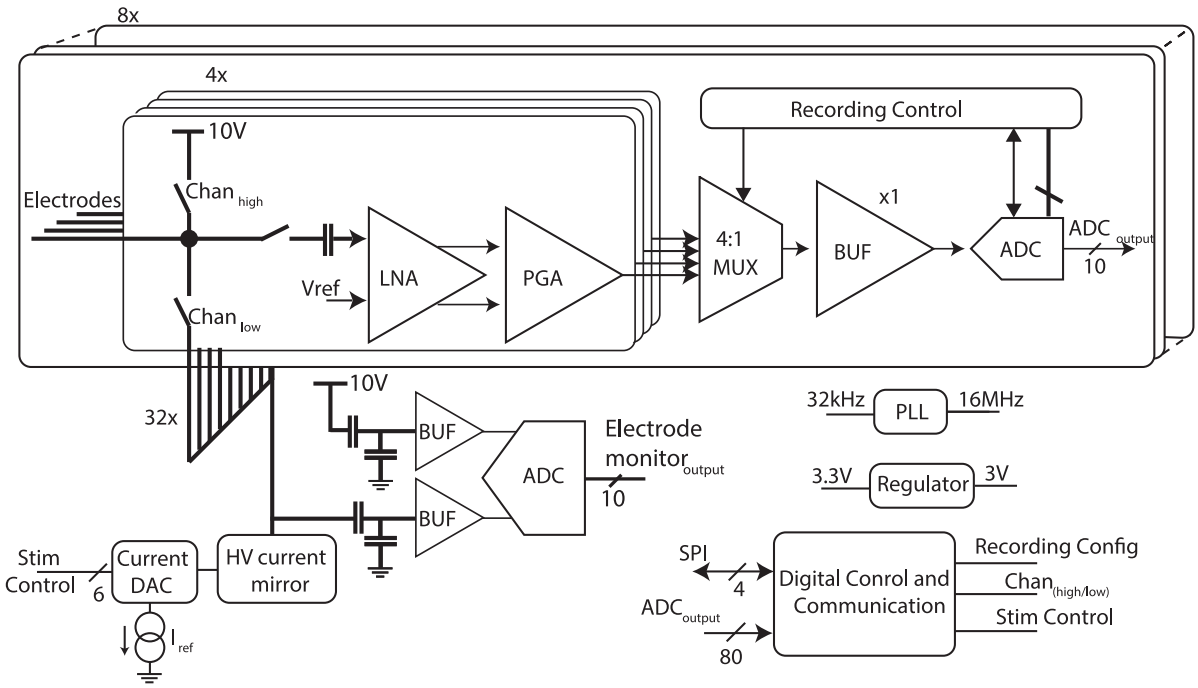

Fig. 2. ASIC architecture. 32 parallel neural recording channels, grouped in blocks of four, sharing an ADC. A single current control block combined with a 32-channel H-bridge controls the flow of stimulation current. Also shown are the digital communication and control; and ancillary support (LDO and PLL).

Array (FPGA) and a variety of power receiving and conversion circuitry and a clock source for the chip. The SenseBack ASIC was designed to be highly flexible, low-power, and small to enable implantable bidirectional neural interfacing. Fig. 1(e) shows the bare die, which measures 3.9 $\times$ 3.9 mm. It was packaged in an 8 $\times$ 8 mm 64 pin QFN carrier.

1) Neural Interface Node: The chip, whose architecture is shown in Fig 2, provides 32 bidirectional channels, each capable of high voltage stimulation and electromyography (EMG) and neural recording. The analog stages of the neural recording front-end and ADC was presented in [31]. The recording channels are arranged in groups of four, with each group sharing a 10-bit Analogue to Digital Converter (ADC) sampling at 80 kHz (each at 20 kHz). Recording channels have a programmable gain of between 225 and 4725. Low-pass filter settings allow the cutoff of each channel to be set at either 280 Hz or 5 kHz. The high-pass filter settings offer greater granularity – a 0.05 Hz fixed filter at the input is combined with a configurable analog high-pass filter (global 5-bit control between 30–600 Hz) and a per group digital filter (nine steps between 5 Hz and 1765 Hz). Each channel can be set to bypass the global and digital high pass filters to enable recording of very low frequency signals, e.g. local field potentials. Each recording channel is also capable of working in a spike detection mode whereby the channel only outputs data for 16 samples around a user configurable absolute value threshold crossing. This windowing of the data reduces the data rate, by two orders of magnitude, and hence the data transmission power.

The chip is capable of bipolar, biphasic, current-controlled stimulation across any pair of the 32 channels with a voltage compliance of 10 V. The current is controlled by a combination of a 6-bit digital to analog converter (DAC) and a multiplier stage which amplifies the current five or 50 times. Utilising the low multiplier setting, the current is controlled in 500 nA steps up to 31.5 μA, whereas with the high gain setting the steps are 5 μ up to 315 μA. The system is designed to produce stimuli in batches (of between 1 and 256), described in stimulation configurations. Each configuration identifies: the various parameters of an individual stimulation; the number of repetitions to perform; an initial inter-stimulation interval; and finally a "ramp" parameter which allows the inter-stimulus interval to be automatically shortened/lengthened to easily create a ramp in the frequency of action potentials generated. Thirty two of these stimulation configurations can be stored in memory and each can be triggered by a single 16-bit command sent to the chip. This approach of storing stimulation profiles on-chip enables highly accurate inter-stimulus interval control, while also greatly reducing the uplink data rate, that is one data word can trigger 256 stimuli with a smoothly changing stimulation frequency and associated power consumption. More information on stimulation control was reported in [6].

The chip I/Os are: (i) the 32 channels; (ii) a reference channel for neural recording; (iii) a low frequency 32.768 kHz clock; (iv) a Serial Peripheral Interface (SPI); an interrupt request pin for control and data readout; and (v) three power supplies (3.3, 10, and 20 V). The low voltage supplies the vast majority of the analogue and digital circuitry. The 10 V supply powers the stimulation circuitry and the 20 V simply allows safe biasing of various nodes to avoid issues associated with voltage doubling by the H-bridge [32].

The ASIC is SPI master and clocks the bus at approximately 16 MHz (multiplied with a Phase Locked Loop from the low frequency clock). The ASIC output is event driven (i.e. active

whenever data is ready to send), while for system control an external system can request communication by toggling the interrupt request pin.

2) Wireless interface node: The SenseBack implant has a wireless transceiver that can receive commands for stimulation control and transmit data recorded from the nervous system. Typically the power requirements for a multi-channel neural interface can be prohibitively large. Data reductions made possible by the SenseBack ASIC as well as the likely redundancy of some recording channels, make it possible to use low data rate and power wireless protocols although this does limit the number of channels of raw data that can be streamed simultaneously. Following a review of commercially available wireless microcontrollers, the low power Nordic NRF52832 was chosen on the basis of its ability to provide the highest data rates available over Bluetooth Low Energy 5 (2 Mbps on the physical layer) and its availability in small packages. The only downside being that the 2.4 GHz band is sub-optimal for transcutaneous transmission. Ultimately the fully integrated (including a 0.6 dBi antenna) 8×8 mm ISP1507 System in Package was chosen (Fig. 1(c)).

A small and low power FPGA (Fig. 1(c)) was added as an interface between the microcontroller and the ASIC to buffer the high data rate output from the ASIC. A Lattice ICE5 LP4K chip was chosen due to its extremely small size and low power consumption and our previous experience, including research demonstrating its suitability for spike sorting [unpublished], as an alternative to the Igloo Nano FPGA, which we used in [33]. However, as currently implemented, this FPGA simply acts as a transparent high speed buffer, enabling both the MCU and the ASIC to communicate as master over SPI at different frequencies. As a slave device the FPGA can initiate data transmissions by toggling a request line to either the MCU or ASIC as appropriate.

The FPGA can load its firmware either from non-volatile programming memory that can only be written once, or its volatile memory can be programmed. We desired maximum system flexibility and as such we included the FPGA image into the microcontroller program and set up the microcontroller to bitbang program the FPGA at boot time. This flexibility was further extended by modifying a Nordic Semiconductor provided bootloader. The bootloader was designed to search for firmware updates over Bluetooth for 10 seconds, before loading the main program. This enables the microcontroller, and hence the FPGA, to be reprogrammed wirelessly even after encapsulation and implantation.

Wireless data communication with a PC is conducted via a dongle (Fig. 1(f)) over the Bluetooth 5 protocol, with the implant acting in a peripheral role and as a GATT server. The link utilises the 2 Mbps physical layer with Data Link Extensions and notifications to maximise the data throughput. Benchtop measurements of throughput indicated that transfer speeds of up to 1.3 Mbps are possible.

3) Wireless Power and Power Conversion: Transcutaneous power transfer is achieved using a commercial inductive wireless power system consisting of a transmitter (P9235A-R and coil – Fig. 1(e)) in the backpack and receiver (P9027LP-R and coil) in the implant. The main drivers for these component choices were size and potential efficiency at light loads. The vast majority of commercial ICs for wireless power transfer are for substantially higher power transfer rates (for charging mobile device batteries) and efficiencies at very light loads are poor. The P9235A-R and P9027LP-R were identified as offering acceptable efficiency and very compact implementations, especially for the size-critical receiver. The chosen power transfer ICs operate at a relatively low frequency (kHz range), which trades off some transfer efficiency for reduced impact on tissue from absorption heating [34]. The system was tuned in accordance with the manufacturers recommendations with assumed loads of between 10–100 mW.

B. Encapsulation

The mammalian body is a hostile place for electronics and protecting them for the target six month implantation period within such tight space constraints remains a challenge. A review of the literature identified several previously used biocompatible encapsulants including a variety of silicones, epoxies and parylene-C [35]–[39]. Polymeric approaches for non-hermetic encapsulation were investigated. Several options were tested before settling on silicone Med-6215 as the preferred encapsulant. Hermetic packaging was not considered due to expected size, weight, cost and wireless transmission issues. The encapsulation process utilised for the final devices involved 3 main steps: 1) careful cleaning involving 30 minute ultrasound baths in Acetone, Isopropyl Alcohol and De-Ionised (DI) water followed by oven baking to dry; 2) suspending the device in a mould and dispensing the silicone under partial vacuum to minimise air entrapment, Fig. 3; and 3) following dispensing, atmospheric pressure was restored, the supports were removed and curing was carried out as recommended by the manufacturer (+30 min at 150 ^{o}C).

C. Backpack

The rat backpack inductively provides transcutaneous power to the implant. Here the P9235A-R wireless power transmitter was combined with a 15 mm diameter transmitter coil (SWA15T15H20C01B) 70 mAh Lithium Polymer battery (ASR00011) and the charging electronics from a USB battery pack. Together these components create a USB rechargeable, wireless power transmission module.

III. Experimental Methods and Results

The system was tested in a series of bench, *ex-vivo* and *in-vivo* experiments. All animal care and procedures were performed under appropriate licences issued by the UK Home office under the Animals (Scientific Procedures) Act (1986) and were approved by the Animal Welfare and Ethical Review Board of Imperial College London for *ex-vivo experiments* or that of Newcastle University for *in-vivo* experiments.

1) Bench Testing: The core functionality of the system was validated in a series of bench tests. Firstly the linearity of the stimulator was measured using a resistor (270 kΩ for the low and 27 kΩ for the high current settings) and the resulting waveforms were averaged on an oscilloscope over 10 stimuli. The results are shown in Fig. 4(a)–(b) and demonstrate accurate control of

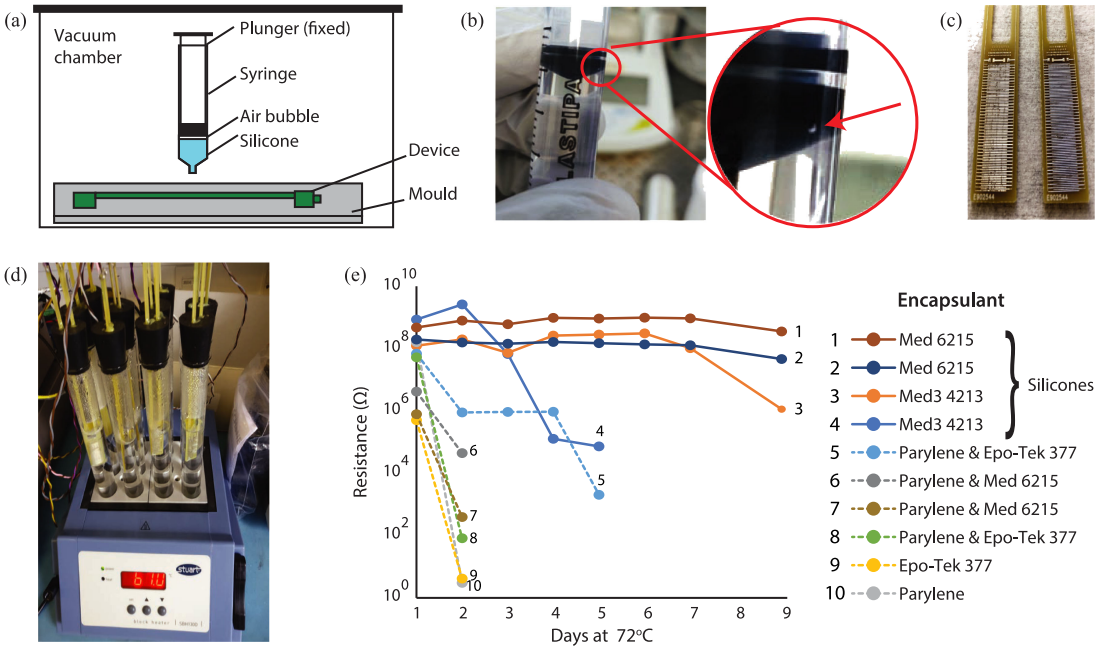

Fig. 3. Partial vacuum silicone dispensing. (a). Silicone filled syringe suspended above the mould in a vacuum chamber; (b). An example air bubble in the silicone syringe which will expand under vacuum and force the silicone out. (c). Example interdigitated test devices used for encapsulation testing; (d). Saline filled test tubes containing encapsulated test devices with 5 V potential difference between tracks being heated for accelerated aging testing; (e). Impedance changes over time for interdigitated test devices encapsulated in a variety of materials.

stimulation current across both the high and low 6-bit stimulation ranges, demonstrating differential and integral non-linearity of less than 1 Least Significant Bit (LSB).

The ability of the system to record μV level signals, filter them and digitally transmit the data was tested using an arbitrary waveform generator (set to generate sine wave frequency sweeps) and a potential divider with a gain of $\frac{1}{100}$. An in-depth assessment of the analogue front-end was performed on a companion IC that shared the same design (see [31] for further details). Once this had been confirmed the ability of the system to perform spike detection, peak alignment, and snippet streaming, was tested with the same setup, but with the waveform generator generating spike shapes. The captured waveform snippets are shown in Fig. 4(c).

For the evaluation of wireless communication, first a throughput test was performed at various ranges in office environment, resulting in a maximum measured throughput of 1.3 Mbps. Then the wireless signal strength of the implant in various orientations was measured in a quieter, but unshielded environment under 2 conditions: (1) unobstructed, and (2) with the implant inserted $>$5 mm deep in a piece of meat. The resulting lobe pattern can be seen in Fig. 4(d)–(f) and indicate that the system has no obvious nulls, but experiences approximately 20 dB attenuation when inside tissue.

The thermal performance of the unencapsulated system was measured using a thermal camera. The system was powered through inductive charging and set to stream data out wirelessly at its maximum rate. The resulting thermal images of the hindlimb and scruff nodes are shown in Fig. 4(h)–(i), indicating a hotspot on the small wireless power receiver chip.

Power consumption testing was performed using a multimeter in low-pass filtered ammeter mode using pre-production boards with identical components to the final implant board. The results of which are shown in Fig. 4(j), indicating system power consumption of between 17 and 78 mW. The system power consumption shows an overall power consumption reduction of approximately 70% (from 79 mW down to 21 mW) when recording on all 32 channels using spike windowing versus recording just 4 channels of raw data – highlighting both the potential of the spike windowing approach and the impact of data bandwidth on system power consumption.

Finally Wireless power transfer measurements, with well aligned coils and a 1 mm spacer, indicated that the transfer efficiency (total input over total output power) was between 1.6-13.7% (under light-heavy load).

2) Encapsulation Testing: Parylene-C, an epoxy (EPO-TEK 377) and 2 silicones (NuSil MED-6215 and MED3-4213) were tested for encapsulation. The testing was performed using planar, interdigitated test boards [40]. Two boards were cleaned and then coated in each of the four test materials and combinations of parylene-C and epoxy or silicone. Dip or pour coating was used for the epoxy and silicones. Chemical vapour deposition was used to apply a 1.5 μm thick parylene-C coat. The encapsulated test samples were then placed in heated saline for accelerated aging testing [41]. A temperature of 72 ^{o}C was chosen, giving an approximate acceleration factor of 11.3. An automated test system based on a 10 channel Keithley 7158 Low Current Scanner combined with a Keithley 7001 Switch System and Keithley 6430 Sub-femtoamp Sourcemeter was used to apply a 5 V DC bias to all the samples and then sequentially remove the bias and test the resistance between the two nodes of each sample device. Testing for each sample was ceased once its resistance dropped below 1 MΩ. The result of the exploratory analysis are shown in Fig. 3(e) and indicate that the epoxy and

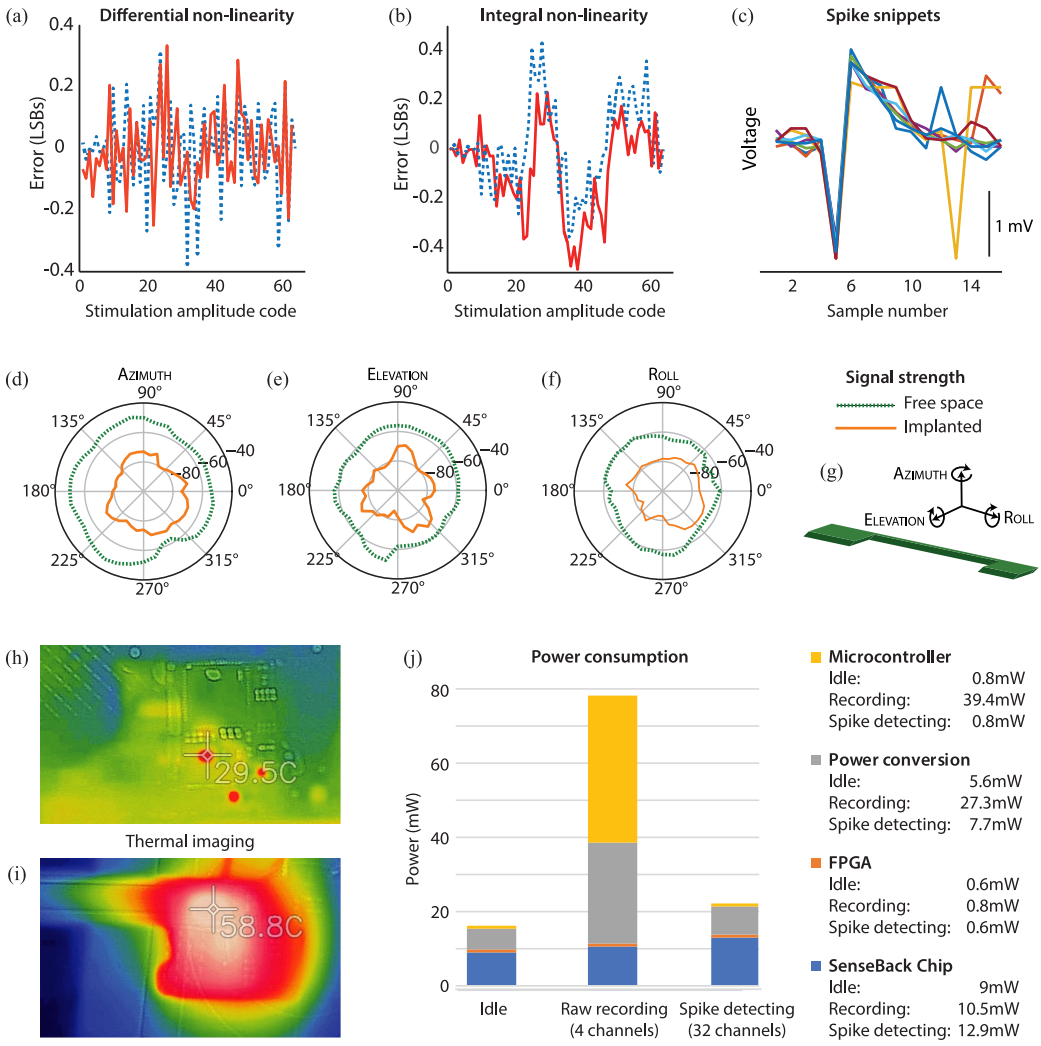

Fig. 4. Bench testing results. (a) and (b). Differential and integral non-linearity of the stimulator; blue, dotted lines represent low amplitude stimulation and red lines high amplitude stimulation; (c). Peak aligned spike snippets output by the SenseBack chip from an arbitrary waveform generator; (d)–(f). Wireless communication signal strength coverage maps at 1 m distance with the device implanted 5 mm deep in tissue using the built in 0.6 dBi antenna and a transmit strength of 0 dBm; (g). Orientations for the wireless signal strength testing; (h) and (i). Thermal images of the unencapsulated implant (hindlimb and scruff end respectively); (j). Power consumption under different usage scenarios.

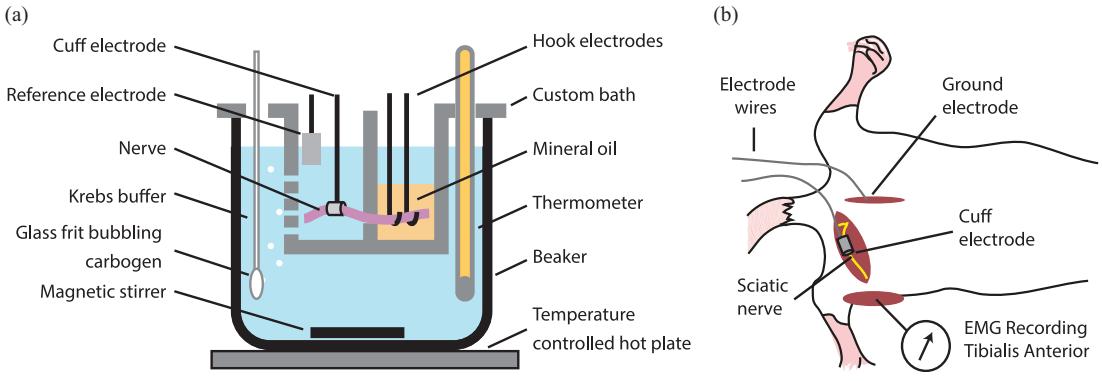

Fig. 5. Diagrams of the test setups: (a) *ex-vivo* preparation showing an extracted nerves placed in custom bath with a nerve cuff on one end for stimulation and Ag-AgCl hook for recording. Mineral oil was used as insulation; (b)*in-vivo* setup showing the positioning of the nerve cuff and recording EMG electrodes.

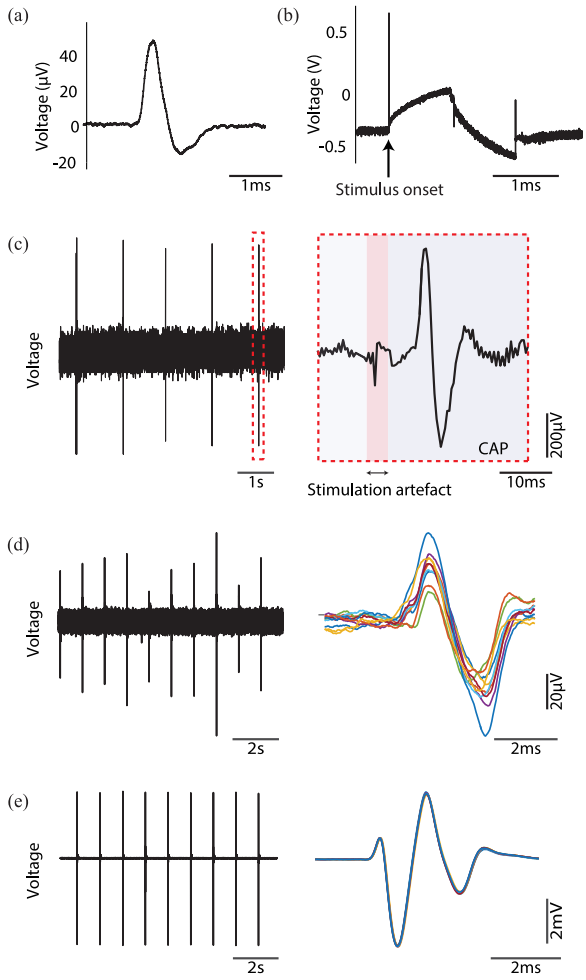

Fig. 6. *Ex-vivo* and *in-vivo results*. (a) and (b). Oscilloscope recordings from *ex-vivo* stimulation testing, showing a compound action potential (CAP) in A and stimulation pulse voltage waveform recorded at the electrodes in (b); (c). *Ex-vivo* recordings from the SenseBack system of a train of CAPs from a series of 5 stimuli at 1 s apart and the enlargement of dotted section, a single stimulation showing the stimulation artefact and subsequent CAP; (d) and (e). *In-vivo* recordings of EMG responses evoked with the SenseBack system at EMG threshold (d) and maximal muscle stimulation (e). Response trains are shown on the left and peak-aligned responses are shown on the right.

parylene-C coatings rapidly failed, while the silicones lasted substantially longer with some lasting the full 9 days – estimated to be equivalent to 100 days at 37 ^{o}C.

3) Ex-Vivo Testing: Sciatic nerves from Sprague Dawley rats were removed, cleaned and placed in a 2-chamber custom bath, as shown in Fig. 5(a). This bath allowed one end of the nerve to be in temperature controlled, oxygenated Krebs buffer, while the other end was isolated electrically in mineral oil. Cuff electrodes for stimulation were placed around the nerve in aqueous solution while Ag-AgCl hook electrodes were used for recording in mineral oil (see [42] for more information on the experimental setup). Fig. 6(a)–(b) show the system stimulating a Compound Action Potential (CAP) in the nerve and the associated waveform across the electrodes during the stimulation. Fig. 4(c) shows the neural recording capture of a CAP spike train (and a zoom in showing the CAP in more detail and associated stimulation artefact).

4) In-Vivo Testing: Two Sprague Dawley rats were used in this study weighing approximately 450 g. Anaesthesia was initially induced in a box with 3% isoflurane in Oxygen. The animal was then moved onto a surgical table where anaesthesia was maintained with a nose cone. Anaesthetic level was adjusted as required throughout the experiment to maintain anaesthesia depth. A tail vein cannula delivered fluid (20 ml 0.9% NaCl and 5% glucose, with 0.05 ml KCl) at 0.2 ml/hour.

An incision was made in the skin approximately 1 cm caudal and parallel to the femur. The muscle tissue was then dissected to expose the sciatic nerve. A nerve cuff was implanted on the sciatic nerve. Silicone sealant (Kwik-Cast, World Precision Instruments, FL, USA) was applied around the cuffs to secure them in place. With a second incision we exposed the Tibialis Anterior muscle. The EMG signal was recorded via a pair of tungsten wires using a Cerebus system (BlackRock Microsystems, USA). Another incision was made over the L6 spinous process. The ground electrode for recordings was a tungsten wire, which was wrapped around L6 and secured with dental acrylic. All openings were covered in saline and gauze to keep the tissue wet while the rest of the procedure was carried out. More details can be found in [27], [28]. Fig. 5 shows the animal preparation.

To date *in-vivo* trials have been limited to acute proofs-of-concept, involving graded neural stimulation and EMG recording. The sciatic nerve was stimulated with the SenseBack and BlackRock CereStim systems, for comparison, via the cuff electrode. In an initial testing the SenseBack system showed a muscle response threshold at much lower levels than the CereStim. Subsequent investigation showed that including 1 kΩ resistors in the stimulation path removes this discrepancy. Fig. 6(d), (e). show the SenseBack system evoking EMG signals in a controlled and repeatable manner at both threshold and maximal levels.

IV. Concluding Remarks

The goal of the work presented here was to develop an implantable neural interface to support a range of chronic neuroscience experiments investigating artificial sensation in small animals. The proposed SenseBack system is a highly versatile neural interface platform and could offer new levels of implanted capability and functionality. This paper highlights and presents novel solutions to a number of important challenges that arise in developing implants for rodent electrophysiology and for translating neural interface research chips into full wireless setups appropriate for bidirectional interfacing with the nervous system.

Space is highly constrained in implants – larger devices present greater surgical and animal welfare challenges, and may necessitate the use of larger animals which increases ethical and financial concerns. When discrete components are used to design implants then there is a clear trade-off between functionality (in terms of stimulation and recording channels) and size. Previous designs, such as [23]–[25] which are detailed in Table I), offered low numbers of either stimulation and/or recording channels. However, having both stimulation and recording capability greatly increases experimental options and a high channel count increases the odds that one of the electrodes will be well positioned to interface to target neurons.

TABLE I
COMPARISON OF FULLY IMPLANTABLE RODENT NEURAL INTERFACES

	Shon *et al.* [23]	Paralikar *et al.* [24]	Xu *et al.* [25]	Lee *et al.* [26]	This work
# recording channels	2	0	0	32	32
# stim. channels	2	4	2	4	32
Recording gain	40-120dB	n/a	n/a	52-76dB	47-73dB
Recording bitdepth	12	n/a	n/a	10	9
Stimulation step:max [μA]	20:1500	25:2500	10 mV:3 V	60:1860	0.5:31.5 + 5:315
Stimulation compliance	3.3 V	unknown	3 V	1 V	10 V
Power source	Inductive + secondary	Inductive + secondary	Inductive	Inductive	Inductive
Power consumption [mW]	19.9-82.5 †		0-20‡	18.5△	17-78▲
Packaging	Photo-polymer	Titanium	Silicone	Silicone + Epoxy	Silicone
Dimensions [mm]	33×28×12	37×16.5×6	22×23×7	30×15×5	13.5×12×3 + 12.7×14×3
Volume	~11cm^3	~3cm^3	~3.5cm^3	~2.3cm^3	~1.5cm^3
Weight	21 g	6 g	3.8 g	2.8 g	11.9 g◇

† Idle-worst case power consumption whilst recording.
‡ Idle-worst case stimulator power consumption (external controller 86–320 mW).
△ Nominal power consumption.
▲ Idle-worst case power consumption whilst recording.
◇ Unencapsulated weight 1.2 g. Backpack weight is estimated at circa 6 g, although battery size may need to be increased to extend system operation time.

Besides, it could offer a greater range and control of sensations elicited potentially. This work therefore focused on delivering a high channel count interface and delivered excellent space efficiency by making each of the channels highly flexible and bidirectional. The resulting system is capable of recording neural and muscular activity as well as accurately driving small and large stimulation currents (for intrafascicular and extrafascicular electrodes respectively).

Powering a fully implanted device remains a challenging prospect. Implanted primary batteries for a chronic experiment would be too large, so inductive transcutaneous power is typically used (possibly in conjunction with an implanted secondary battery). However, transcutaneous power transfer is often inefficient and the waste energy is dissipated as heat which can be damaging to the surrounding tissue. Numerous papers attempted to address the efficiency issues, e.g. [43], [44], however, none of these approaches are readily available for laboratory testing. An alternative approach to reducing the energy wasted in transmission, is to address the implant power consumption. The SenseBack ASIC was designed to be a power efficient neural interface chip and to support system wide power savings by reducing the uplink and downlink data rate. The spike windowing approach can reduce the data rate by orders of magnitude (with a concomitant system power reduction) and enabled the use of a low power and commercially available wireless data link.

The long term vision of the SenseBack project remains fixed on enhancing the functionality and acceptability of prosthetic limbs, forbidirectional neural interfacing is a key enabler. At the outset of the project the best approach to delivering a revolutionary prosthetic limb in the near term was judged to be an implanted bidirectional electrical neural interface. In the intervening time, however, significant progress was made in a number of alternative technologies. In particular, work into non-invasive or minimally invasive decoding of limb movement both in the periphery and the central nervous system is a highly active field [45]–[48] and offers the major advantage of requiring no implanted components. Also, in closed-loop applications, other methods such as optogenetics [49], [50] and magnetic recording [51], [52] can potentially address the limitation of electrical interfacing with the neural and muscular systems.

Looking to the future, there are a number of ongoing and planned and activities that could address known issues with the current system and further enhance it to explore some of the exciting future prospects identified. In the near-term we will look at mitigating thermal performance by reducing power consumption using software updates (e.g. microcontroller power consumption could be reduced by as much approximately 15 mW by reducing transmission power strength at the expense of transmission range and this would cause a concomitant reduction in power consumption in the voltage conversion circuitry) and duty cycling. This will be supplemented by further measurements of the total thermal output of the tiny (2.2 × 3.6 mm) wireless power receiver which shows as a hotspot in the thermal imaging and combined with modelling of the systems thermal impact on the surrounding tissue (both conducted and absorbed RF energy) to better understand tissue damage concerns. In the longer term we would like to investigate real-time spike sorting [33] and closed loop stimulation using the onboard FPGA, and create a further iteration of the ASIC and system to: improve the stimulation flexibility; address the current steering spikes; and develop a custom wireless power transmission system. We also intend to investigate the ability of the system to drive LEDs for use in optogenetic experiments.

ACKNOWLEDGMENT

The authors would like to thank Jack Pearson for his help with the silicone encapsulation.

REFERENCES

[1] K. Nazarpour, Ed., *Control Prosthetic Hands: Emerging Avenues Challenges*. London, U.K.: IET, London, 2020, to be published.
[2] D. J. Tyler, "Creating a prosthetic hand that can feel," *IEEE Spectr.*, vol. 53, no. 5, pp. 24–29, 2016.
[3] J. Charthad *et al.*, "A mm-sized wireless implantable device for electrical stimulation of peripheral nerves," *IEEE Trans. Biomed. Circuits Syst.*, vol. 12, no. 2, pp. 257–270, Apr. 2018.

[4] H. T. Lancashire, D. Jiang, A. Demosthenous, and N. Donaldson, "An ASIC for recording and stimulation in stacked microchannel neural interfaces," *IEEE Trans. Biomed. Circuits Syst.*, vol. 13, no. 2, pp. 259–270, Apr. 2019.

[5] C. E. Larson and E. Meng, "A review for the peripheral nerve interface designer," *J. Neurosci. Methods*, p. 108523, 2019.

[6] I. Williams, A. Rapeaux, Y. Liu, S. Luan, and T. G. Constandinou, "A 32-ch. bidirectional neural/EMG interface with on-chip spike detection for sensorimotor feedback," in *Proc. IEEE Biomed. Circuits Syst. Conf.*, 2016, pp. 528–531.

[7] T. Pistohl, D. Joshi, G. Ganesh, A. Jackson, and K. Nazarpour, "Artificial proprioceptive feedback for myoelectric control," *IEEE Trans. Neural Syst. Rehabil. Eng.*, vol. 23, no. 3, pp. 498–507, May 2015.

[8] E. K. Brunton, C. Silveira, J. Rosenberg, M. A. Schiefer, J. Riddell, and K. Nazarpour, "Temporal modulation of the response of sensory fibers to paired-pulse stimulation," *IEEE Trans. Neural Syst. Rehabil. Eng.*, vol. 27, no. 9, pp. 1676–1683, Sep. 2019.

[9] K. Famm, B. Litt, K. J. Tracey, E. S. Boyden, and M. Slaoui, "Drug discovery: A jump-start for electroceuticals," *Nature*, vol. 496, no. 7444, p. 159, 2013.

[10] S. Stanslaski *et al.*, "A chronically implantable neural coprocessor for investigating the treatment of neurological disorders," *IEEE Trans. Biomed. Circuits Syst.*, vol. 12, no. 6, pp. 1230–1245, Dec. 2018.

[11] A. Zhou *et al.*, "A wireless and artefact-free 128-channel neuromodulation device for closed-loop stimulation and recording in non-human primates," *Nature Biomed. Eng.*, vol. 3, no. 1, pp. 15–26, 2019.

[12] P. Olofsson and C. Bouton, "Bioelectronic medicine: An unexpected path to new therapies," *J. Internal Med.*, vol. 286, no. 3, pp. 237–239, 2019.

[13] J. R. Fritz and J. M. Huston, "Advances in bioelectronic medicine: Noninvasive electrical, ultrasound and magnetic nerve stimulation," *Bioelectron. Med.*, vol. 2, no. 4, pp. 143–150, 2019.

[14] D. J. Weber, R. Friesen, and L. E. Miller, "Interfacing the somatosensory system to restore touch and proprioception: Essential considerations," *J. Motor Behav.*, vol. 44, no. 6, pp. 403–418, 2012.

[15] H. P. Saal and S. J. Bensmaia, "Biomimetic approaches to bionic touch through a peripheral nerve interface," *Neuropsychologia*, vol. 79, pp. 344–353, 2015.

[16] M. Aman *et al.*, "Experimental testing of bionic peripheral nerve and muscle interfaces: Animal model considerations," *Front. Neurosci.*, vol. 13, p. 1442, 2020.

[17] C. Günter, J. Delbeke, and M. Ortiz-Catalan, "Safety of long-term electrical peripheral nerve stimulation: Review of the state of the art," *J. Neuroeng. Rehabil.*, vol. 16, no. 1, p. 13, 2019.

[18] C. Russell, A. D. Roche, and S. Chakrabarty, "Peripheral nerve bionic interface: A review of electrodes," *Int. J. Intell. Robot. Appl.*, vol. 3, no. 1, pp. 11–18, 2019.

[19] P. Gutruf and J. A. Rogers, "Implantable, wireless device platforms for neuroscience research," *Current Opinion Neurobiol.*, vol. 50, pp. 42–49, 2018.

[20] G. Gagnon-Turcotte, Y. LeChasseur, C. Bories, Y. Messaddeq, Y. De Koninck, and B. Gosselin, "A wireless headstage for combined optogenetics and multichannel electrophysiological recording," *IEEE Trans. Biomed. Circuits Syst.*, vol. 11, no. 1, pp. 1–14, Feb. 2016.

[21] B. Lee *et al.*, "An inductively-powered wireless neural recording and stimulation system for freely-behaving animals," *IEEE Trans. Biomed. Circuits Syst.*, vol. 13, no. 2, pp. 413–424, Apr. 2019.

[22] N. H. Kazmers, A. T. Fragomen, and S. R. Rozbruch, "Prevention of pin site infection in external fixation: A review of the literature," *Strategies Trauma Limb Reconstruct.*, vol. 11, no. 2, pp. 75–85, 2016.

[23] A. Shon, J.-U. Chu, J. Jung, H. Kim, and I. Youn, "An implantable wireless neural interface system for simultaneous recording and stimulation of peripheral nerve with a single cuff electrode," *Sensors*, vol. 18, no. 1, p. 1, 2018.

[24] K. Paralikar *et al.*, "A fully implantable and rechargeable neurostimulation system for animal research," in *Proc. 7th Int. IEEE/EMBS Conf. Neural Eng.*, 2015, pp. 418–421.

[25] Q. Xu, D. Hu, B. Duan, and J. He, "A fully implantable stimulator with wireless power and data transmission for experimental investigation of epidural spinal cord stimulation," *IEEE Trans. Neural Syst. Rehabil. Eng.*, vol. 23, no. 4, pp. 683–692, Jul. 2015.

[26] B. Lee *et al.*, "An implantable peripheral nerve recording and stimulation system for experiments on freely moving animal subjects," *Sci. Rep.*, vol. 8, no. 1, p. 6115, 2018.

[27] E. Brunton, C. W. Blau, and K. Nazarpour, "Separability of neural responses to standardised mechanical stimulation of limbs," *Sci. Rep.*, vol. 7, no. 1, pp. 1–14, 2017.

[28] C. Silveira, E. Brunton, S. Spendiff, and K. Nazarpour, "Influence of nerve cuff channel count and implantation site on the separability of afferent ENG," *J. Neural Eng.*, vol. 15, no. 4, p. 046004, 2018.

[29] C. Silveira *et al.*, "W:ti flexible transversal electrode array for peripheral nerve stimulation: A feasibility study," Aug. 2020.

[30] I. Williams *et al.*, "Senseback–implant considerations for an implantable neural stimulation and recording device," in *Proc. IEEE Biomed. Circuits Syst. Conf.*, 2019, pp. 1–4.

[31] Y. Liu, S. Luan, I. Williams, A. Rapeaux, and T. G. Constandinou, "A 64-channel versatile neural recording SoC with activity-dependent data throughput," *IEEE Trans. Biomed. Circuits Syst.*, vol. 11, no. 6, pp. 1344–1355, Dec. 2017.

[32] I. Williams and T. G. Constandinou, "An energy-efficient, dynamic voltage scaling neural stimulator for a proprioceptive prosthesis," *IEEE Trans. Biomed. Circuits Syst.*, vol. 7, no. 2, pp. 129–139, Apr. 2013.

[33] S. Luan *et al.*, "Compact standalone platform for neural recording with real-time spike sorting and data logging," *J. Neural Eng.*, vol. 15, no. 4, p. 046014, 2018.

[34] N. Soltani, M. S. Aliroteh, M. T. Salam, J. L. P. Velazquez, and R. Genov, "Low-radiation cellular inductive powering of rodent wireless brain interfaces: Methodology and design guide," *IEEE Trans. Biomed. Circuits Syst.*, vol. 10, no. 4, pp. 920–932, Aug. 2016.

[35] T. Stieglitz, "Manufacturing, assembling and packaging of miniaturized neural implants," *Microsyst. Technol.*, vol. 16, no. 5, pp. 723–734, 2010.

[36] F. Boeser, J. S. Ordonez, M. Schuettler, T. Stieglitz, and D. T. Plachta, "Non-hermetic encapsulation for implantable electronic devices based on epoxy," in *Proc. 37th Annu. Int. Conf. IEEE Eng. Med. Biol. Soc.*, 2015, pp. 809–812.

[37] C. Hassler, T. Boretius, and T. Stieglitz, "Polymers for neural implants," *J. Polym. Sci. Part B: Polym. Phys.*, vol. 49, no. 1, pp. 18–33, 2011.

[38] B. Gosselin *et al.*, "A mixed-signal multichip neural recording interface with bandwidth reduction," *IEEE Trans. Biomed. Circuits Syst.*, vol. 3, no. 3, pp. 129–141, Jun. 2009.

[39] A. Vanhoestenberghe, N. Donaldson, N. Lovell, and G. Suaning, "Hermetic encapsulation of an implantable vision prosthesis-combining implant fabrication philosophies," in *Proc. 13th Int. FES Soc. Conf.*, 2008, pp. 187–189.

[40] J.-M. Hsu, L. Rieth, R. A. Normann, P. Tathireddy, and F. Solzbacher, "Encapsulation of an integrated neural interface device with Parylene C," *IEEE Trans. Biomed. Eng.*, vol. 56, no. 1, pp. 23–29, Jan. 2008.

[41] D. Hukins, A. Mahomed, and S. Kukureka, "Accelerated aging for testing polymeric biomaterials and medical devices," *Med. Eng. Phys.*, vol. 30, no. 10, pp. 1270–1274, 2008.

[42] A. Rapeaux and T. G. Constandinou, "A block-capable and module-extendable 4-channel stimulator for acute neurophysiology," *J. Neural Eng.*, to be published, doi: 10.1101/2020.01.28.923474.

[43] G. Wang, W. Liu, M. Sivaprakasam, and G. A. Kendir, "Design and analysis of an adaptive transcutaneous power telemetry for biomedical implants," *IEEE Trans. Circuits Syst. I: Reg. Papers*, vol. 52, no. 10, pp. 2109–2117, Oct. 2005.

[44] M. Kiani, U.-M. Jow, and M. Ghovanloo, "Design and optimization of a 3-coil inductive link for efficient wireless power transmission," *IEEE Trans. Biomed. Circuits Syst.*, vol. 5, no. 6, pp. 579–591, Dec. 2011.

[45] F. V. Tenore, A. Ramos, A. Fahmy, S. Acharya, R. Etienne-Cummings, and N. V. Thakor, "Decoding of individuated finger movements using surface electromyography," *IEEE Trans. Biomed. Eng.*, vol. 56, no. 5, pp. 1427–1434, May 2008.

[46] S. Waldert *et al.*, "Hand movement direction decoded from MEG and EEG," *J. Neurosc.*, vol. 28, no. 4, pp. 1000–1008, 2008.

[47] M. Dyson, J. Barnes, and K. Nazarpour, "Myoelectric control with abstract decoders," *J. Neural Eng.*, vol. 15, no. 5, p. 056003, 2018.

[48] M. Dyson, S. Dupan, H. Jones, and K. Nazarpour, "Learning, generalization, and scalability of abstract myoelectric control," *IEEE Trans. Neural Syst. Rehabil. Eng.*, vol. 28, no. 7, pp. 1539–1547, 2020.

[49] C. Towne, K. L. Montgomery, S. M. Iyer, K. Deisseroth, and S. L. Delp, "Optogenetic control of targeted peripheral axons in freely moving animals," *PloS One*, vol. 8, no. 8, 2013.

[50] F. Michoud *et al.*, "Optical cuff for optogenetic control of the peripheral nervous system," *J. Neural Eng.*, vol. 15, no. 1, p. 015002, 2018.

[51] S. Zuo, H. Heidari, D. Farina, and K. Nazarpour, "Miniaturized magnetic sensors for implantable magnetomyography," *Adv. Mater. Technol.*, vol. 5, no. 6, p. 2000185, 2020.

[52] S. Zuo *et al.*, "Ultrasensitive magnetoelectric sensing system for pico-Tesla magnetomyography," *IEEE Trans. Biomed. Circuits Syst.*, to be published, doi: 10.1109/TBCAS.2020.2998290.